MOX-Report No. 65/2022

Mixed Virtual Element approximation of linear acoustic wave equation

Dassi, F.; Fumagalli, A.; Mazzieri, I.; Vacca, G.

Mixed Virtual Element approximation of linear acoustic wave equation

FRANCO DASSI

Dipartimento di Matematica e Applicazioni, Università degli Studi di Milano Bicocca, Via R. Cozzi, 55, 20125, Milano, Italy

ALESSIO FUMAGALLI

MOX - Dipartimento di Matematica, Politecnico di Milano, P.za L. da Vinci, 32, 20133, Milano, Italy

ILARIO MAZZIERI*

MOX - Dipartimento di Matematica, Politecnico di Milano, P.za L. da Vinci, 32, 20133, Milano, Italy

AND

GIUSEPPE VACCA

Dipartimento di Matematica, Università degli Studi di Bari, via E. Orabona, 4, 70125, Bari, Italy
*Corresponding author: ilario.mazzieri@polimi.it

We design a Mixed Virtual Element Method for the approximated solution to the first-order form of the acoustic wave equation. In absence of external load, the semi-discrete method exactly conserves the system energy. To integrate in time the semi-discrete problem we consider a classical θ-method scheme. We carry out the stability and convergence analysis in the energy norm for the semi-discrete problem showing optimal rate of convergence with respect to the mesh size. We further study the property of energy conservation for the fully-discrete system. Finally, we present some verification tests as well as engineering application of the method.

Keywords: Mixed Virtual Elements; acoustics wave equations; polygonal meshes; energy conservation.

1. Introduction

The numerical simulation of acoustic, elastic or electromagnetic wave propagation finds application in many scientific disciplines, including aerospace, geophysics, civil engineering, telecommunications, and medicine for instance.

The present work considers a Mixed Virtual Element method on general polytopal grids for the discretization of the acoustic wave equation written as a first order system of hyperbolic partial differential equations.

In general, mixed methods consider the discretization of vector fields in some $H(\mathrm{div})$-conforming spaces while scalar fields in some L^2 spaces. Classes of mixed methods include the well known Raviart-Thomas (RT) [9, 58, 61], the Brezzi-Douglas-Marini (BDM) [26, 30, 31, 56] finite element schemes and more recently the Mixed Virtual Element Methods (MVEM) [15, 39]. The VEM, introduced firstly in [14], have been applied recently to various differential problems, including elasticity [10], Stokes [20, 33], Navier-Stokes [21], Cahn-Hilliard [2], Darcy [39], Helmholtz [53], Maxwell [18] and wave [4, 40, 62] equations.

The major benefit of using VEM, instead of classical approaches, is the fact that it gives the opportunity to preserve at the discrete level some important properties valid at the continuous level. In particular, it is possible to design discrete spaces with global high regularity, which preserve the

polynomial divergence/curl, that are robust with respect to mesh-locking phenomena. Moreover, VEM can handle general polytopal meshes, that are particularly useful to account for small features in the model (such as cracks, holes and inclusions), and treat in an automatic way hanging nodes, movable meshes and adaptivity.

The very first analysis of RT finite element discretization applied for the spatial approximation of the acoustic wave equation is presented by Geveci in [46]. He showed that even if the RT finite elements conserve the energy of the system, when a time discretization is applied, the fully-discrete method produces an implicit time-marching scheme which is inefficient, since the mass matrix is nondiagonal. For this reason it is preferred to use mass lumping techniques, see e.g. [13, 37] or symplectic schemes that conserve a positive-definite perturbed energy functional [52]. A slightly different formulation, in which two time derivatives appear on the vector variable and none on the other equation has been analysed in literature, see, for instance, [34, 38, 49, 50, 51].

Discontinuous Galerkin (dG) methods have been also considered for the solution of the wave equation in the mixed form, see for instance [11, 34, 35, 36, 55]. However, they have been mostly studied for the second order hyperbolic version: we mention [48, 60] for the scalar case, [5, 8, 42, 43, 44, 54, 59] for the vectorial case and [3, 6, 7] where a dG approximation on polygonal grids is considered. Within the framework of polytopal methods we mention a recent work by [32] where the Hybrid High-Order (HHO) method is applied to the wave equation in either first and second order form and [19] where the Mimetic Finite Differences is applied in the context of Hamiltonian wave equations.

Here, for the first time, a MVEM is considered for the solution of linear wave acoustics written as a system of first order partial differential equations. The analysis is carried out by taking inspiration from the approaches proposed in [17, 22] and [39]. Concerning the choice of the degrees of freedom, the proposed scheme can be seen as the extension on polytopal grids of RT finite elements. The integration in time of the semi-discrte problem is achieved by considering a θ-method scheme.

The paper is organised as follows: in Section 2 we review the mathematical model, its weak formulation, a stability result and the energy conservation of the system. In Section 3 after introducing the virtual element spaces with the associated set of degrees of freedom and defining the discrete bilinear forms, we present the semi-discrete virtual element formulation and establish the well-posedness of the semi-discrete problem, the stability bound for discrete solution in a discrete energy norm and the energy conservation. In Section 4 we analyse the theoretical properties of the proposed method: by considering the Fortin operator introduced in [39], we recall the interpolation estimates. Then, we prove optimal order of convergence for the proposed method. Moreover we estimate the error between the energy of the exact solution and the energy of the virtual element solution. In Section 5 we introduce the family of θ-method schemes for integrating in time the semidiscrete problem in Section 3.4 and discuss the property of energy conservation. In Section 6 we provide some experiments to give numerical evidence of the behaviour of the proposed scheme. Finally, Section 7 is devoted to conclusions and future perspectives.

Notations and Preliminaries

Throughout the paper we will follow the usual notation for Sobolev spaces and norms as in [1]. Let $\Omega \subset \mathbb{R}^2$ be the computational domain with Lipschitz continuous boundary $\partial\Omega$ and external unit normal $\boldsymbol{n}$, we denote with $\boldsymbol{x} = (x_1, x_2)$ the independent variable. With a usual notation the symbols ∇ and curl denote the gradient and curl for scalar functions, while div denotes the divergence operator for vector fields. For an open bounded domain ω, the norm in the space $L^p(\omega)$ is denoted by $\|\cdot\|_{L^p(\omega)}$, norm and seminorm in $H^s(\omega)$ are denoted respectively by $\|\cdot\|_{s,\omega}$ and $|\cdot|_{s,\omega}$, while $(\cdot,\cdot)_\omega$ and $\|\cdot\|_{0,\omega}$ denote the

L^2-inner product and the L^2-norm (the subscript ω may be omitted when ω is the whole computational domain Ω).

We recall the following well known functional spaces which will be useful in the sequel

$$H(\mathrm{div}, \omega) := \{ \mathbf{v} \in [L^2(\omega)]^2 : \mathrm{div}\, \mathbf{v} \in L^2(\omega) \},$$

$$H(\mathrm{curl}, \omega) := \{ \mathbf{v} \in [L^2(\omega)]^2 : \mathrm{curl}\, \mathbf{v} \in L^2(\omega) \},$$

and introduce the following spaces

$$\mathbf{V} := \{ \mathbf{v} \in H(\mathrm{div}, \Omega) \quad \text{s.t.} \quad \mathbf{v} \cdot \mathbf{n} = 0 \text{ on } \Gamma_N \}, \quad Q := L^2(\Omega),$$

where $\Gamma_N \subset \partial\Omega$, equipped with natural inner products and induced norms.

Since we are dealing with a time dependent problem, we will also consider the following Bochner spaces. Let $T > 0$, for space-time functions $v(\mathbf{x}, t)$ defined on $\omega \times (0, T)$, we denote with v_t the derivative with respect to the time variable. Furthermore, using standard notations [57], for a Banach space V with norm $\| \cdot \|_V$, we introduce the space

$$L^2(0, T; V) := \left\{ v \colon (0, T) \to V \text{ s.t. } v \text{ measurable}, \int_0^T \| v(t) \|_V^2 dt < +\infty \right\}.$$

In similar way, for $n \geq 0$, we consider the space $C^n(0, T; V)$.

2. Mathematical Model

Let $\Omega \subset \mathbb{R}^2$ be the polygonal domain. The boundary $\partial\Omega$ is divided in three parts, with mutually disjoint interiors, denoted by Γ_D, Γ_N and Γ_R, corresponding to Dirichlet, Neumann and Robin boundary conditions, respectively; one or two of them may be empty.

In a time interval $(0, T]$, for a piece-wise constant positive real valued function c (representing the characteristic velocity of the medium), and a scalar source f, the following problem is set in Ω.

Problem 1 (Model problem) *Find $(\mathbf{u}, p)$ such that*

$$\begin{cases} \mathbf{u}_t(\mathbf{x}, t) - \nabla p(\mathbf{x}, t) = \mathbf{0} \\ c^{-2} p_t(\mathbf{x}, t) - \mathrm{div}\, \mathbf{u}(\mathbf{x}, t) = f(\mathbf{x}, t) \end{cases} \quad \text{in } \Omega \times (0, T],$$

supplied with the following boundary conditions

$$\begin{cases} p(\mathbf{x}, t) = g_D(\mathbf{x}, t) & \text{on } \Gamma_D \times (0, T], \\ \mathbf{u}(\mathbf{x}, t) \cdot \mathbf{n} = g_N(\mathbf{x}, t) & \text{on } \Gamma_N \times (0, T], \\ \mathbf{u}(\mathbf{x}, t) \cdot \mathbf{n} + \alpha^{-1} c^{-1} p(\mathbf{x}, t) = g_R(\mathbf{x}, t) & \text{on } \Gamma_R \times (0, T], \end{cases}$$

being $\alpha > 0$ an impedance parameter, and g_D, g_N and g_R given functions, and initial conditions

$$\begin{cases} p(\mathbf{x}, 0) = p_0(\mathbf{x}) & \text{in } \Omega, \\ \mathbf{u}(\mathbf{x}, 0) = \mathbf{u}_0(\mathbf{x}) & \text{in } \Omega. \end{cases}$$

This problem describes the space-time variation of particle velocity $\boldsymbol{u}$ and acoustic pressure p in a heterogeneous medium where waves propagate with characteristic velocity $c = \sqrt{\frac{\mu}{\rho}}$, being $\rho > 0$ the density and $\mu > 0$ the viscosity of the medium, respectively. Notice that the condition on $\Gamma_R \times [0,T]$ is known in the literature as impedance boundary condition and includes the low-order absorbing condition when $\alpha = 1$ and $g_R = 0$, [11]. In the following we suppose $\boldsymbol{u}_0 \in Q^2$, $p_0 \in Q$, $f \in L^2(0,T;Q)$ and for the sake of presentation we set $g_D = g_N = g_R = 0$ and $\alpha = 1$. The general case, i.e., with non-homogeneous boundary conditions con be treated similarly. Next, we define the following bilienar forms

$$
\begin{aligned}
m(\cdot,\cdot)\colon \boldsymbol{V} \times \boldsymbol{V} \to \mathbb{R} \qquad & m(\boldsymbol{u},\boldsymbol{v}) := (\boldsymbol{u},\boldsymbol{v})_\Omega \qquad && \forall (\boldsymbol{u},\boldsymbol{v}) \in \boldsymbol{V} \times \boldsymbol{V}, \\
n(\cdot,\cdot)\colon Q \times Q \to \mathbb{R} \qquad & n(p,q) := (c^{-2}p,q)_\Omega \qquad && \forall (p,q) \in Q \times Q, \\
b(\cdot,\cdot)\colon \boldsymbol{V} \times Q \to \mathbb{R} \qquad & b(\boldsymbol{u},q) := (\operatorname{div}\boldsymbol{u},q)_\Omega \qquad && \forall (\boldsymbol{u},q) \in \boldsymbol{V} \times Q, \\
r(\cdot,\cdot)\colon \boldsymbol{V} \times \boldsymbol{V} \to \mathbb{R} \qquad & r(\boldsymbol{u},\boldsymbol{v}) := (c\boldsymbol{u}\cdot\boldsymbol{n},\boldsymbol{v}\cdot\boldsymbol{n})_{\Gamma_R} \qquad && \forall (\boldsymbol{u},\boldsymbol{v}) \in \boldsymbol{V} \times \boldsymbol{V},
\end{aligned}
\tag{2.2}
$$

and the linear functional associated to given data is defined as

$$
F(\cdot)\colon Q \to \mathbb{R} \qquad F(q) := (f,q)_\Omega \qquad \forall q \in Q.
$$

Then the weak formulation of Problem 1 reads as follows

Problem 2 (Weak problem) *Find the velocity $\boldsymbol{u} \in L^2(0,T;\boldsymbol{V}) \cap C^0(0,T;Q^2)$, and the pressure $p \in L^2(0,T;Q) \cap C^0(0,T;Q)$ s.t.*

$$
\begin{cases}
m(\boldsymbol{u}_t,\boldsymbol{v}) + b(\boldsymbol{v},p) + r(\boldsymbol{u},\boldsymbol{v}) = 0 \qquad & \forall \boldsymbol{v} \in \boldsymbol{V}, \\
n(p_t,q) - b(\boldsymbol{u},q) = F(q) \qquad & \forall q \in Q,
\end{cases}
$$

with initial condition $\boldsymbol{u}(\cdot,0) = \boldsymbol{u}_0$ and $p(\cdot,0) = p_0$ in Ω.

Using standard arguments is possible to prove that Problem 2 is well posed, [11, 27, 51] and satisfies the following stability estimate, cf. also [45]

$$
\sup_{0 \le t \le T} \|(\boldsymbol{u},p)(t)\|_{\mathscr{E}} \le \int_0^T \|cf(s)\|_{0,\Omega} \, \mathrm{d}s + \|(\boldsymbol{u}_0,p_0)\|_{\mathscr{E}},
$$

where

$$
\|(\boldsymbol{v},q)\|_{\mathscr{E}}^2 := \|\boldsymbol{v}\|_{0,\Omega}^2 + \|c^{-1}q\|_{0,\Omega}^2 \quad \forall (\boldsymbol{v},q) \in [L^2(\Omega)]^2 \times Q.
\tag{2.3}
$$

We finally observe that if $f = 0$ and $\Gamma_R = \emptyset$ Problem 2 is energy conservative, i.e. the solution $(\boldsymbol{u},p)$ of Problem 2 satisfies

$$
\|(\boldsymbol{u},p)(t)\|_{\mathscr{E}} = \|(\boldsymbol{u}_0,p_0)\|_{\mathscr{E}} \qquad \forall t \in [0,T].
\tag{2.4}
$$

3. Mixed Virtual Elements

In this Section we describe the virtual element discretization of Problem 2 on general polygonal meshes. In particular, in Section 3.1 we introduce the assumptions on the regularity of the polygonal meshes together with the definition of crucial projector operators that will be fundamental in the construction of the VE discretization. In Section 3.2 we describe the $H(\operatorname{div})$-conforming VE spaces, whereas in

Section 3.3 we present the discrete forms. Finally, in Section 3.4 we introduce the semi-discrete VE discretization of Problem 2 and we provide the stability bound of the solution and the energy preserving property of the semi-discrete system.

3.1. *Mesh assumptions and polynomial projections*

From now on, we will denote by E a general polygon having ℓ_E edges e. For each polygon E and each edge e of E we denote by $|E|$, h_E the measure and diameter of E respectively, by h_e we denote the length of e. Furthermore $\boldsymbol{n}_E^e$ (resp. $\boldsymbol{n}_E$) denotes the unit outward normal vector to e (resp. to ∂E).

Let $\{\Omega_h\}_h$ be a sequence of decompositions of Ω into general polygons E, where the granularity h is defined as $h = \sup_{E \in \Omega_h} h_E$. We suppose that $\{\Omega_h\}_h$ fulfills the following assumption:

(A1) Mesh assumption. There exists a positive constant ρ such that for any $E \in \{\Omega_h\}_h$

- Any $E \in \{\Omega_h\}_h$ is star-shaped with respect to a ball B_E of radius $\geq \rho\, h_E$;
- Any edge e of any $E \in \{\Omega_h\}_h$, $h_e \geq \rho\, h_E$.

We remark that the hypotheses above, though not too restrictive in many practical cases, could possibly be further relaxed, combining the present analysis with the studies in [23, 24, 28].

Referring to Problem 2, we assume that for any h the decomposition Ω_h matches with the subdivision of $\partial\Omega$ into Γ_D, Γ_N, Γ_R and with the definition of the piece-wise constant velocity c. We denote by Σ_h the set of all the mesh edges and, for any $E \in \Omega_h$, we define Σ_h^E the set of the edges of E. The total number of vertexes, edges and elements in the decomposition Ω_h are denoted by L_V, L_e and L_P, respectively.

Using standard VE notations, for any mesh object $\omega \in \Omega_h \cup \Sigma_h$ and for any $n \in \mathbb{N}$ let us introduce the space $\mathbb{P}_n(\omega)$ to be the space of polynomials defined on ω of degree $\leq n$, with the extended notation $\mathbb{P}_{-1}(\omega) = \{0\}$. For any $n \in \mathbb{N}$ and for any non-negative $s \in \mathbb{R}$ we consider the broken spaces

- $\mathbb{P}_n(\Omega_h) = \{q \in L^2(\Omega) \quad \text{s.t.} \quad q|_E \in \mathbb{P}_n(E) \quad \text{for all } E \in \Omega_h\}$,
- $H^s(\Omega_h) = \{v \in L^2(\Omega) \quad \text{s.t.} \quad v|_E \in H^s(E) \quad \text{for all } E \in \Omega_h\}$,

equipped with the broken norm and seminorm

$$\|v\|_{H^s(\Omega_h)}^2 = \sum_{E \in \Omega_h} \|v\|_{H^s(E)}^2, \qquad |v|_{H^s(\Omega_h)}^2 = \sum_{E \in \Omega_h} |v|_{H^s(E)}^2.$$

For any $E \in \Omega_h$, let us introduce the $\boldsymbol{L^2}$**-projection** $\Pi_n^{0,E} \colon L^2(E) \to \mathbb{P}_n(E)$, given by

$$\int_E q_n (v - \Pi_n^{0,E} v)\, \mathrm{d}E = 0 \qquad \text{for all } v \in L^2(E) \text{ and } q_n \in \mathbb{P}_n(E),$$

with obvious extension for vector functions $\Pi_n^{0,E} \colon [L^2(E)]^2 \to [\mathbb{P}_n(E)]^2$. The global counterpart $\Pi_n^0 \colon L^2(\Omega_h) \to \mathbb{P}_n(\Omega_h)$, is defined for all $E \in \Omega_h$ by

$$(\Pi_n^0 v)|_E = \Pi_n^{0,E} v. \tag{3.1}$$

In the following the symbol $\lesssim$ will denote a bound up to a generic positive constant, independent of the mesh size h and of the time step τ introduced in Section 5, but which may depend on Ω, on the "polynomial" order k and on the regularity constant appearing in the mesh Assumption **(A1)**.

3.2. *Virtual Element spaces*

We start by presenting an overview of the $H(\mathrm{div})$-conforming Virtual Element space, cf. [15, 16, 39].

Let $k \geq 0$ be the "polynomial" order of the method. We thus consider on each polygonal element $E \in \Omega_h$ the virtual space

$$\boldsymbol{V}_k(E) = \left\{ \boldsymbol{v} \in H(\mathrm{div}, E) \cap H(\mathrm{curl}, E) \text{ s.t. } (i) \ \mathrm{div}\,\boldsymbol{v} \in \mathbb{P}_k(E), \right.$$

$$(ii) \ \mathrm{curl}\,\boldsymbol{v} \in \mathbb{P}_{k-1}(E),$$

$$\left. (iii) \ (\boldsymbol{v} \cdot \boldsymbol{n}_E^e)|_e \in \mathbb{P}_k(e) \ \forall e \in \Sigma_h^E \right\}.$$

In the following, we summarize the main properties of the space $\boldsymbol{V}_k(E)$. We refer to [15, 16, 39] for a detailed analysis.

(P1) **Polynomial inclusion:** $\mathbb{P}_k(E) \subseteq \boldsymbol{V}_k(E)$;

(P2) **Degrees of freedom:** the following linear operators $\mathbf{D_V}$ constitute a set of DoFs for $\boldsymbol{V}_k(E)$: for any $\boldsymbol{w} \in \boldsymbol{V}_k(E)$ we consider

$\mathbf{D_V}1$ the element moments of the divergence

$$\int_E (\mathrm{div}\,\boldsymbol{w})\, p_k \, \mathrm{d}E \qquad \forall p_k \in \mathbb{P}_k(E) \setminus \mathbb{R},$$

$\mathbf{D_V}2$ the element moments

$$\int_E \boldsymbol{w} \cdot (p_{k-1}\boldsymbol{x}^\perp) \, \mathrm{d}E \qquad \forall p_k \in \mathbb{P}_{k-1},$$

where $\boldsymbol{x}^\perp := (y, -x)^{\mathrm{T}}$;

$\mathbf{D_V}3$ the edge moments

$$\int_e (\boldsymbol{w} \cdot \boldsymbol{n}_E^e)\, p_k \, \mathrm{d}e \qquad \forall p_k \in \mathbb{P}_k(e), \ \forall e \in \Sigma_h^E.$$

Therefore the dimension of $\boldsymbol{V}_k(E)$ is

$$\dim(\boldsymbol{V}_k(E)) = \ell_E\,(k+1) + k^2 + 2k.$$

(P3) **Computable quantities:** for any $\boldsymbol{w} \in \boldsymbol{V}_k(E)$ the DoFs $\mathbf{D_V}$ allow to compute

$$\Pi_k^{0,E}\boldsymbol{w}, \qquad \mathrm{div}\,\boldsymbol{w}, \qquad (\boldsymbol{w} \cdot \boldsymbol{n}_E^e)|_e \quad \forall e \in \Sigma_h^E.$$

The global virtual element space $\boldsymbol{V}_k$ is defined by gluing together all local spaces, that is: we require that for any internal edge $e \in \Sigma_h^E \cap \Sigma_h^{E'}$, shared by E and E',

$$\boldsymbol{w}|_E \cdot \boldsymbol{n}_E^e + \boldsymbol{w}|_{E'} \cdot \boldsymbol{n}_{E'}^e = 0 \qquad \forall \boldsymbol{w} \in \boldsymbol{V}_k,$$

that is in accordance with the DoFs definition $\mathbf{D_V}1$. Therefore we have

$$\boldsymbol{V}_k := \{\boldsymbol{v} \in \boldsymbol{V} \quad \text{s.t.} \quad \boldsymbol{v}|_E \in \boldsymbol{V}_k(E) \ \forall E \in \Omega_h\}. \tag{3.2}$$

The dimension of $\boldsymbol{V}_k$ is thus given by

$$\dim(\boldsymbol{V}_k) = (k+1)L_e + (k^2+2k)L_P\,.$$

The discrete pressure space Q_k is given by the piecewise polynomial functions of degree k, i.e.

$$Q_k := \mathbb{P}_k(\Omega_h)\,. \tag{3.3}$$

3.3. *Virtual Element forms*

The next step in the construction of our method is the definition of a discrete version of the continuous forms in (2.2). Following the usual procedure in the VE setting, we need to construct discrete forms that are computable through the DoFs. Notice that in the light of property **(P3)**, for any $\boldsymbol{v}_h, \boldsymbol{w}_h \in \boldsymbol{V}_k$ and $q_h, p_h \in Q_k$ the quantities

$$n(p_h, q_h), \qquad b(\boldsymbol{v}_h, q_h), \qquad r(\boldsymbol{v}_h, \boldsymbol{w}_h), \qquad F(q_h)$$

are computable.

Whereas for arbitrary functions in $\boldsymbol{V}_k$ the form $m(\cdot, \cdot)$ is not computable since the discrete functions are not known in closed form. Employing property **(P3)** for any $\boldsymbol{v}_h, \boldsymbol{w}_h \in \boldsymbol{V}_k(E)$ we define the computable local discrete bilinear form:

$$m_h^E(\boldsymbol{v}_h, \boldsymbol{w}_h) := \int_E (\Pi_k^{0,E}\boldsymbol{v}_h) \cdot (\Pi_k^{0,E}\boldsymbol{w}_h)\,\mathrm{d}E + h_E^{-2}\mathscr{S}^E(\boldsymbol{v}_h, \boldsymbol{w}_h)\,. \tag{3.4}$$

The stabilizing term in (3.4) is given by

$$\mathscr{S}^E(\boldsymbol{v}_h, \boldsymbol{w}_h) = S^E\big((I - \Pi_k^{0,E})\boldsymbol{v}_h,\, (I - \Pi_k^{0,E})\boldsymbol{w}_h\big)\,,$$

where $S^E(\cdot, \cdot)\colon \boldsymbol{V}_k(E) \times \boldsymbol{V}_k(E) \to \mathbb{R}$ is a computable symmetric discrete form. In the present paper we consider the so-called `dofi-dofi` stabilization [14] defined as follows: let $\vec{\boldsymbol{v}}_h$ and $\vec{\boldsymbol{w}}_h$ denote the real valued vectors containing the values of the local degrees of freedom (properly scaled) associated to $\boldsymbol{v}_h$, $\boldsymbol{w}_h$ in the space $\boldsymbol{V}_k(E)$ then

$$S^E(\boldsymbol{v}_h, \boldsymbol{w}_h) = \vec{\boldsymbol{v}}_h \cdot \vec{\boldsymbol{w}}_h\,.$$

Under mesh Assumption **(A1)** the form $S^E(\cdot, \cdot)$ satisfies the following bounds (we refer to [39] for the details)

$$\|\boldsymbol{v}_h\|_{0,E}^2 \lesssim h_E^2 S^E(\boldsymbol{v}_h, \boldsymbol{v}_h) \lesssim \|\boldsymbol{v}_h\|_{0,E}^2\,, \tag{3.5}$$

for all $\boldsymbol{v}_h \in \boldsymbol{V}_k(E) \cap \ker(\Pi_k^{0,E})$.

The global form $m_h(\cdot, \cdot)\colon (\boldsymbol{V}_k \cup [\mathbb{P}_k(\Omega_h)]^2) \times (\boldsymbol{V}_k \cup [\mathbb{P}_k(\Omega_h)]^2) \to \mathbb{R}$ can be derived adding the local contributions

$$m_h(\boldsymbol{v}_h, \boldsymbol{w}_h) := \sum_{E \in \Omega_h} m_h^E(\boldsymbol{v}_h, \boldsymbol{w}_h) \qquad \forall (\boldsymbol{v}_h, \boldsymbol{w}_h) \in (\boldsymbol{V}_k \cup [\mathbb{P}_k(\Omega_h)]^2)\,. \tag{3.6}$$

Notice that, from (3.4) and (3.5), it follows that

$$m_h(\boldsymbol{p}_k, \boldsymbol{v}_h) = m(\boldsymbol{p}_k, \boldsymbol{v}_h) \qquad\qquad \forall \boldsymbol{p}_k \in [\mathbb{P}_k(\Omega_h)]^2\,, \boldsymbol{v}_h \in (\boldsymbol{V}_k \cup [\mathbb{P}_k(\Omega_h)]^2)\,, \tag{3.7}$$

$$\|\boldsymbol{v}_h\|_{0,\Omega}^2 \lesssim m_h(\boldsymbol{v}_h, \boldsymbol{v}_h) \lesssim \|\boldsymbol{v}_h\|_{0,\Omega}^2 \qquad\qquad \forall \boldsymbol{v}_h \in (\boldsymbol{V}_k \cup [\mathbb{P}_k(\Omega_h)]^2)\,. \tag{3.8}$$

3.4. *Virtual Element semi-discrete problem*

Referring to the spaces (3.2) and (3.3), the forms (2.2) and the discrete bilinear form (3.6), we can state the following semi-discrete problem.

Problem 3 (VEM problem) *Find $\boldsymbol{u}_h \in L^2(0,T;\boldsymbol{V}_k) \cap C^0(0,T;Q^2)$, and $p_h \in L^2(0,T;Q_k) \cap C^0(0,T;Q_k)$ s.t.*

$$\begin{cases} m_h(\boldsymbol{u}_{h_t}, \boldsymbol{v}_h) + b(\boldsymbol{v}_h, p_h) + r(\boldsymbol{u}_h, \boldsymbol{v}_h) = 0 & \forall \boldsymbol{v}_h \in \boldsymbol{V}_k, \\ n(p_{h_t}, q_h) - b(\boldsymbol{u}_h, q_h) = F(q_h) & \forall q_h \in Q_k, \end{cases}$$

with initial condition $\boldsymbol{u}_h(\cdot, 0) = \Pi_k^0 \boldsymbol{u}_0$ and $p_h(\cdot, 0) = \Pi_k^0 p_0$ in Ω.

The well-posedness of Problem 3 follows from:

- discrete inf-sup condition [16]: there exists $\widehat{\beta} > 0$ s.t.

$$\inf_{q_h \in Q_k} \sup_{\boldsymbol{v}_h \in \boldsymbol{V}_k} \frac{b(\boldsymbol{v}_h, q_h)}{\|\boldsymbol{v}_h\|_{\boldsymbol{V}} \|q_h\|_Q} \geq \widehat{\beta}.$$

- coercivity on the discrete kernel: the bilinear form $m_h(\cdot, \cdot)$ satisfies

$$m_h(\boldsymbol{v}_h, \boldsymbol{v}_h) \gtrsim \|\boldsymbol{v}_h\|_{\boldsymbol{V}}^2 \qquad \forall \boldsymbol{v}_h \in \boldsymbol{K}_k,$$

where $\boldsymbol{K}_k := \{\boldsymbol{v}_h \in \boldsymbol{V}_k \quad \text{s.t.} \quad b(\boldsymbol{v}_h, q_h) = 0 \ \forall q_h \in Q_k\}$.

Let us introduce the discrete energy norm

$$\|(\boldsymbol{v}_h, q_h)\|_{\mathscr{E}_h}^2 := m_h(\boldsymbol{v}_h, \boldsymbol{v}_h) + \|c^{-1} q_h\|_{0,\Omega}^2 \quad \forall (\boldsymbol{v}_h, q_h) \in (\boldsymbol{V}_k \cup [\mathbb{P}_k(\Omega_h)]^2) \times Q_k. \qquad (3.9)$$

Then, using analogous argument to that used for the continuous case, the discrete solution $(\boldsymbol{u}_h, p_h)$ of Problem 3 satisfies the following stability estimate

$$\sup_{0 \leq t \leq T} \|(\boldsymbol{u}_h, p_h)(t)\|_{\mathscr{E}_h} \leq \int_0^T \|c f(s)\|_{0,\Omega} \, \mathrm{d}s + \|(\Pi_k^0 \boldsymbol{u}_0, \Pi_k^0 p_0)\|_{\mathscr{E}},$$

where, from (3.7), we have used that

$$\|(\boldsymbol{p}_k, q_h)\|_{\mathscr{E}_h} = \|(\boldsymbol{p}_k, q_h)\|_{\mathscr{E}} \qquad \forall (\boldsymbol{p}_k, q_h) \in [\mathbb{P}_k(\Omega_h)]^2 \times Q_k.$$

Furthermore if $f = 0$ and $\Gamma_R = \emptyset$, Problem 3 is energy conservative, i.e. the solution $(\boldsymbol{u}_h, p_h)$ of Problem 3 satisfies

$$\|(\boldsymbol{u}_h, p_h)(t)\|_{\mathscr{E}_h} = \|(\Pi_k^0 \boldsymbol{u}_0, \Pi_k^0 p_0)\|_{\mathscr{E}} \qquad \forall t \in [0, T], \qquad (3.10)$$

that is the semi-discrete counterpart of (2.4).

Remark 1 *Notice that definitions (2.3) and (3.9) and bounds (3.8) imply the following norm equivalence*

$$\|(\boldsymbol{v}_h, q_h)\|_{\mathscr{E}} \lesssim \|(\boldsymbol{v}_h, q_h)\|_{\mathscr{E}_h} \lesssim \|(\boldsymbol{v}_h, q_h)\|_{\mathscr{E}} \qquad \forall (\boldsymbol{v}_h, q_h) \in \boldsymbol{V}_k \times Q_k. \qquad (3.11)$$

Remark 2 *The proposed approach can be easily extended to more general situations such as the three dimensional case [15], and domains with curved boundary/interfaces [39, 41]. The analysis could be developed with very similar arguments to the ones in the forthcoming sections.*

4. Theoretical analysis

In this section, we present some theoretical results for the virtual element Problem 3. In Section 4.1 we review the interpolation estimates, whereas in Section 4.2 and Section 4.3 we provide the convergence analysis and the energy error estimate respectively.

4.1. *Interpolation estimates*

We now recall the optimal approximation properties for the space $\boldsymbol{V}_k$ (see [39]). We define the linear Fortin operator $\Pi_k^F \colon [H^1(\Omega)]^2 \to \boldsymbol{V}_k$ in the following way. For any $\boldsymbol{w} \in [H^1(\Omega)]^2$ and for all $e \in \Sigma_h$ and $E \in \Omega_h$, $\Pi_k^F \boldsymbol{w}$ is determined by

$$\int_E \mathrm{div}(\boldsymbol{w} - \Pi_k^F \boldsymbol{w}) \, p_k \, \mathrm{d}E = 0 \quad \forall p_k \in \mathbb{P}_k(E) \setminus \mathbb{R},$$

$$\int_E \mathrm{curl}(\boldsymbol{w} - \Pi_k^F \boldsymbol{w}) \, p_{k-1} \, \mathrm{d}E = 0 \quad \forall p_{k-1} \in \mathbb{P}_{k-1}(E),$$

$$\int_e (\boldsymbol{w} - \Pi_k^F \boldsymbol{w}) \cdot \boldsymbol{n}^e \, p_k \, \mathrm{d}e = 0 \quad \forall p_k \in \mathbb{P}_k(e).$$

The conditions above implies that the following diagram is commutative, i.e.,

$$
\begin{array}{ccccc}
[H^1(\Omega)]^2 & \xrightarrow{\ \mathrm{div}\ } & Q & \xrightarrow{\ 0\ } & 0 \\
{\scriptstyle \Pi_k^F} \downarrow & & {\scriptstyle \Pi_0^k} \downarrow & & \\
\boldsymbol{V}_k & \xrightarrow{\ \mathrm{div}\ } & Q_k & \xrightarrow{\ 0\ } & 0
\end{array}
$$

where 0 is the map that associates to every function the value 0. In particular, for any $\boldsymbol{w} \in [H^1(\Omega)]^2$ it holds (see [39])

$$\mathrm{div}(\Pi_k^F \boldsymbol{w}) = \Pi_k^0 \, \mathrm{div}\,\boldsymbol{w}, \quad \mathrm{curl}(\Pi_k^F \boldsymbol{w}) = \Pi_{k-1}^0 \, \mathrm{curl}\,\boldsymbol{w},$$

$$((\Pi_k^F \boldsymbol{w}) \cdot \boldsymbol{n}^e)|_e = (\Pi_k^{0,e}(\boldsymbol{w} \cdot \boldsymbol{n}^e))|_e \quad \forall e \in \Sigma_h. \tag{4.1}$$

For the Fortin operator we have the following interpolation estimate (see [39, Proposition 4.1]).

Proposition 4.1 (Approximation property of $\boldsymbol{V}_k$) *Under Assumption* **(A1)** *for any* $\boldsymbol{v} \in \boldsymbol{V} \cap [H^s(\Omega_h)]^2$ *where* $1 \le s \le k+1$, $\Pi_F^k \boldsymbol{v}$ *satisfies the estimate*

$$\|\boldsymbol{v} - \Pi_F^k \boldsymbol{v}\|_{0,\Omega} \lesssim h^s |v|_{s,\Omega_h}.$$

We now review a classical approximation result for polynomials on star-shaped domains, see for instance [29].

Lemma 4.1 (Bramble-Hilbert) *Under Assumption* **(A1)** *and referring to* (3.1)*, for all* $q \in H^s(\Omega_h)$ *where* $0 \le s \le k+1$*, it holds*

$$\|q - \Pi_k^0 q\|_{\Omega,0} \lesssim h^s |q|_{\Omega_h,s}.$$

4.2. *Convergence analysis*

In this section we provide the convergence property for the semi-discrete scheme.

Proposition 4.2   *Under Assumption* (**A1**)*, let* $(\boldsymbol{u}, p)$ *be the solution of Problem* 2 *and* $(\boldsymbol{u}_h, p_h)$ *be the solution of Problem* 3*. Assume that*

$$\boldsymbol{u}_t, p_t \in L^1(0, T; H^{k+1}(\Omega_h)) \qquad and \qquad \boldsymbol{u}_0, p_0 \in H^{k+1}(\Omega_h).$$

Then for all $t \in (0, T)$ *the following error estimate holds:*

$$\|(\boldsymbol{u} - \boldsymbol{u}_h, p - p_h)(t)\|_{\mathscr{E}} \lesssim h^{k+1} \left(|\boldsymbol{u}_0|_{k+1, \Omega_h} + \widehat{c}|p_0|_{k+1, \Omega_h} + |\boldsymbol{u}_t|_{L^1(0, t; H^{k+1}(\Omega_h))} + \widehat{c}|p_t|_{L^1(0, t; H^{k+1}(\Omega_h))} \right),$$

where $\widehat{c} := \|c^{-1}\|_{L^\infty(\Omega \times (0, T))}.$

Proof For all $t \in (0, T)$, let us introduce the following error quantities

$$\begin{aligned}
\boldsymbol{e}_I(t) &:= \boldsymbol{u}(t) - \Pi_k^F \boldsymbol{u}(t), & \rho_I(t) &:= p(t) - \Pi_k^0 p(t), \\
\boldsymbol{e}_h(t) &:= \Pi_k^F \boldsymbol{u}(t) - \boldsymbol{u}_h(t), & \rho_h(t) &:= \Pi_k^0 p(t) - p_h(t),
\end{aligned}$$

From triangle inequality and (3.11) it holds

$$\|(\boldsymbol{u} - \boldsymbol{u}_h, p - p_h)(t)\|_{\mathscr{E}} \lesssim \|(\boldsymbol{e}_I, \rho_I)(t)\|_{\mathscr{E}} + \|(\boldsymbol{e}_h, \rho_h)(t)\|_{\mathscr{E}_h}. \tag{4.2}$$

The first term on the right-hand side of (4.2) can be bounded by using Proposition 4.1 and Lemma 4.1 getting

$$\begin{aligned}
\|(\boldsymbol{e}_I, \rho_I)(t)\|_{\mathscr{E}} &\lesssim h^{(k+1)} \left(|\boldsymbol{u}(t)|_{k+1, \Omega_h} + \widehat{c}|p(t)|_{k+1, \Omega_h} \right) \\
&\lesssim h^{k+1} \left(|\boldsymbol{u}_0|_{k+1, \Omega_h} + \widehat{c}|p_0|_{k+1, \Omega_h} + \int_0^t \left(|\boldsymbol{u}_t(s)|_{k+1, \Omega_h} + \widehat{c}|p_t(s)|_{k+1, \Omega_h} \right) \mathrm{d}s \right) \\
&= h^{k+1} \left(|\boldsymbol{u}_0|_{k+1, \Omega_h} + \widehat{c}|p_0|_{k+1, \Omega_h} + |\boldsymbol{u}_t|_{L^1(0, t; H^{k+1}(\Omega_h))} + \widehat{c}|p_t|_{L^1(0, t; H^{k+1}(\Omega_h))} \right).
\end{aligned} \tag{4.3}$$

To estimate the second term on the right-hand side of (4.2) we proceed as follows. We consider Problem 2 and Problem 3 and obtain

$$\begin{aligned}
m(\boldsymbol{u}_t, \boldsymbol{e}_h) + b(\boldsymbol{e}_h, p) + r(\boldsymbol{u}, \boldsymbol{e}_h) + n(p_t, \rho_h) - b(\boldsymbol{u}, \rho_h) &= F(\rho_h), \\
m_h(\boldsymbol{u}_{ht}, \boldsymbol{e}_h) + b(\boldsymbol{e}_h, p_h) + r(\boldsymbol{u}_h, \boldsymbol{e}_h) + n(p_{ht}, \rho_h) - b(\boldsymbol{u}_h, \rho_h) &= F(\rho_h).
\end{aligned}$$

Then subtracting the previous equations we get the following error equation

$$m(\boldsymbol{u}_t, \boldsymbol{e}_h) - m_h(\boldsymbol{u}_{ht}, \boldsymbol{e}_h) + n((p - p_h)_t, \rho_h) + r(\boldsymbol{u} - \boldsymbol{u}_h, \boldsymbol{e}_h) + \eta_b = 0, \tag{4.4}$$

where

$$\eta_b := b(\boldsymbol{e}_h, p - p_h) + b(\boldsymbol{u}_h - \boldsymbol{u}, \rho_h).$$

First, we notice that the term η_b vanishes, in fact

$$
\begin{aligned}
\eta_b &= b(\Pi_k^F \boldsymbol{u}, p - p_h) - b(\boldsymbol{u}_h, p - p_h) + b(\boldsymbol{u}_h, \Pi_k^0 p - p_h) - b(\boldsymbol{u}, \Pi_k^0 p - p_h) \\
&= b(\Pi_k^F \boldsymbol{u}, p - p_h) + b(\boldsymbol{u}, p_h - \Pi_k^0 p) + b(\boldsymbol{u}_h, \Pi_k^0 p - p) \\
&= b(\Pi_k^F \boldsymbol{u}, p - p_h) + b(\boldsymbol{u}, p_h - \Pi_k^0 p) && (\operatorname{div} \boldsymbol{u}_h \in \mathbb{P}_k(\Omega_h) \,\&\, \text{def. } \Pi_k^0) \\
&= b(\Pi_k^F \boldsymbol{u}, p - p_h) + b(\Pi_k^F \boldsymbol{u}, p_h - \Pi_k^0 p) && (p_h - \Pi_k^0 p \in \mathbb{P}_k(\Omega_h) \,\&\, (4.1)) \\
&= b(\Pi_k^F \boldsymbol{u}, p - \Pi_k^0 p) \\
&= 0. && (\operatorname{div}(\Pi_h^F \boldsymbol{u}) \in \mathbb{P}_k(\Omega_h) \,\&\, \text{def. } \Pi_k^0)
\end{aligned}
\tag{4.5}
$$

Therefore, from (4.4) and (4.5) we infer

$$
m_h(\boldsymbol{e}_{h_t}, \boldsymbol{e}_h) + n(\rho_{h_t}, \rho_h) + r(\boldsymbol{e}_h, \boldsymbol{e}_h) = (m_h(\Pi_k^F(\boldsymbol{u}_t), \boldsymbol{e}_h) - m(\boldsymbol{u}_t, \boldsymbol{e}_h)) - n(\rho_{I_t}, \rho_h) - r(\boldsymbol{e}_I, \boldsymbol{e}_h). \tag{4.6}
$$

Recalling that $(\boldsymbol{e}_h \cdot \boldsymbol{n}^e)|_e \in \mathbb{P}_k(e)$ for all $e \in \Sigma_h$, and employing (4.1) we have

$$
r(\boldsymbol{e}_I, \boldsymbol{e}_h) = r(\boldsymbol{u} - \Pi_k^F \boldsymbol{u}, \boldsymbol{e}_h) = 0. \tag{4.7}
$$

Therefore, since $r(\boldsymbol{e}_h, \boldsymbol{e}_h) \geq 0$, from (4.6) and (4.7), and recalling definition (3.9) we obtain

$$
\frac{1}{2} \frac{d}{dt} \|(\boldsymbol{e}_h, \boldsymbol{e}_h)\|_{\mathscr{E}_h}^2 \leq (m_h(\Pi_k^F(\boldsymbol{u}_t), \boldsymbol{e}_h) - m(\boldsymbol{u}_t, \boldsymbol{e}_h)) - n(\rho_{I_t}, \rho_h) =: \eta_{\boldsymbol{u}} + \eta_p. \tag{4.8}
$$

The first term on the right-hand side of the previous equation can be bounded as follows

$$
\begin{aligned}
\eta_{\boldsymbol{u}} &= m_h(\Pi_k^F(\boldsymbol{u}_t) - \Pi_k^0(\boldsymbol{u}_t), \boldsymbol{e}_h) + m(\Pi_k^0(\boldsymbol{u}_t) - \boldsymbol{u}_t, \boldsymbol{e}_h) && (\text{by } (3.7)) \\
&\lesssim (\|\Pi_k^F(\boldsymbol{u}_t) - \Pi_k^0(\boldsymbol{u}_t)\|_{0,\Omega} + \|\boldsymbol{u}_t - \Pi^0(\boldsymbol{u}_t)\|_{0,\Omega}) \|\boldsymbol{e}_h\|_{0,\Omega} && (\text{by } (3.8)) \\
&\lesssim (\|\boldsymbol{u}_t - \Pi_k^F(\boldsymbol{u}_t)\|_{0,\Omega} + \|\boldsymbol{u}_t - \Pi^0(\boldsymbol{u}_t)\|_{0,\Omega}) \|\boldsymbol{e}_h\|_{0,\Omega} && (\text{by tri. ineq.}) \\
&\lesssim h^{k+1} |\boldsymbol{u}_t|_{H^{k+1}(\Omega_h)} m_h(\boldsymbol{e}_h, \boldsymbol{e}_h)^{1/2}
\end{aligned}
\tag{4.9}
$$

where in the last inequality we used Proposition 4.1, Lemma 4.1 and equation (3.8). Whereas η_p is estimated by

$$
\begin{aligned}
\eta_{\boldsymbol{u}} &= n(\Pi^0(p_t) - p_t, \rho_h) \leq \|c^{-1}(\Pi^0(p_t) - p_t)\|_{0,\Omega} \|c^{-1} \rho_h\|_{0,\Omega} \\
&\lesssim \widehat{c} h^{k+1} |p_t|_{H^{k+1}(\Omega_h)} \|c^{-1} \rho_h\|_{0,\Omega}.
\end{aligned}
\tag{4.10}
$$

Therefore recalling definition (3.9), from (4.8), (4.9) and (4.10) and the Cauchy-Schwarz inequality, we obtain

$$
\frac{d}{dt} \|(\boldsymbol{e}_h, \rho_h)(t)\|_{\mathscr{E}_h} \lesssim h^{k+1} \left(|\boldsymbol{u}_t(t)|_{H^{k+1}(\Omega_h)} + \widehat{c} |p_t(t)|_{H^{k+1}(\Omega_h)} \right).
$$

By integrating the previous bound on $(0,t)$ we obtain

$$
\begin{aligned}
\|(\boldsymbol{e}_h, \rho_h)(t)\|_{\mathscr{E}_h} &\lesssim \|(\boldsymbol{e}_h, \rho_h)(0)\|_{\mathscr{E}_h} + h^{k+1} \left(\int_0^t |\boldsymbol{u}_t(s)|_{H^{k+1}(\Omega_h)} \, ds + \widehat{c} \int_0^t |p_t(s)|_{H^{k+1}(\Omega_h)} \, ds \right) \\
&\lesssim \|(\boldsymbol{e}_h, \rho_h)(0)\|_{\mathscr{E}} + h^{k+1} \left(\|\boldsymbol{u}_t\|_{L^1(0,t;H^{k+1}(\Omega_h))} + \widehat{c} \|p_t\|_{L^1(0,t;H^{k+1}(\Omega_h))} \right).
\end{aligned}
\tag{4.11}
$$

We finally bound the initial data error

$$\|(\boldsymbol{e}_h, \rho_h)(0)\|_{\mathscr{E}} \lesssim \|\Pi_k^F \boldsymbol{u}_0 - \Pi_k^0 \boldsymbol{u}_0\|_{0,\Omega} + \widehat{c}\|p_0 - \Pi_k^0 p_0\|_{0,\Omega}$$
$$\lesssim h^{k+1} \left(|\boldsymbol{u}_0|_{H^{k+1}(\Omega_h)} + \widehat{c}\,|p_0|_{H^{k+1}(\Omega_h)} \right). \tag{4.12}$$

The thesis now follows combining (4.11), (4.12) and (4.3) in (4.2). $\quad\square$

4.3. *Energy error*

An important aspect in wave propagation problems is the energy conservation of the continuous and semi-discrete system (cf. (2.4) and (3.10) rispectively). In the following proposition we estimate the errors between the energy of the continuous and the semi-discrete energy of the system.

Proposition 4.3 *Under assuption* **(A1)***, let* $(\boldsymbol{u}, p)$ *be the solution of Problem 2 and* $(\boldsymbol{u}_h, p_h)$ *be the solution of Problem 3 with* $f = 0$ *and* $\Gamma_R = \emptyset$*. Assume that* $\boldsymbol{u}_0, p_0 \in H^{k+1}(\Omega_h)$*. Then for all* $t \in (0, T)$*, the following estimate holds:*

$$0 \le \|(\boldsymbol{u}, p)(t)\|_{\mathscr{E}}^2 - \|(\boldsymbol{u}_h, p_h)(t)\|_{\mathscr{E}_h}^2 \lesssim h^{2(k+1)} \left(|\boldsymbol{u}_0|_{k+1,\Omega_h}^2 + \widehat{c}^2\,|p_0|_{k+1,\Omega_h}^2 \right),$$

where $\widehat{c} := \|c^{-1}\|_{L^\infty(\Omega \times (0,T))}$.

Proof. From (2.4) and (3.10) we infer

$$\|(\boldsymbol{u}, p)(t)\|_{\mathscr{E}}^2 - \|(\boldsymbol{u}_h, p_h)(t)\|_{\mathscr{E}_h}^2 = \|(\boldsymbol{u}_0, p_0)\|_{\mathscr{E}}^2 - \|(\Pi_k^0 \boldsymbol{u}_0, \Pi_k^0 p_0)\|_{\mathscr{E}}^2$$
$$= \|\boldsymbol{u}_0\|_{0,\Omega}^2 + \|\boldsymbol{c}^{-1} p_0\|_{0,\Omega}^2 - \|\boldsymbol{\Pi}_k^0 \boldsymbol{u}_0\|_{0,\Omega}^2 - \|\boldsymbol{c}^{-1} \Pi_k^0 p_0\|_{0,\Omega}^2.$$

Direct application of Pythagorean Theorem yields

$$\|\zeta\|_{0,\Omega}^2 = \|\Pi_k^0 \zeta\|_{0,\Omega}^2 + \|\zeta - \Pi_k^0 \zeta\|_{0,\Omega}^2, \qquad \forall \zeta \in L^2(\Omega),$$

therefore, recalling that c is piece-wise constant w.r.t. Ω_h, we infer

$$\|(\boldsymbol{u}, p)(t)\|_{\mathscr{E}}^2 - \|(\boldsymbol{u}_h, p_h)(t)\|_{\mathscr{E}_h}^2 = \|\boldsymbol{u}_0 - \Pi_k^0 \boldsymbol{u}_0\|_{0,\Omega}^2 + \|c^{-1}(p_0 - \Pi_k^0 p_0)\|_{0,\Omega}^2. \tag{4.13}$$

Then, from (4.13) and Lemma 4.1, the following bounds hold

$$\|(\boldsymbol{u}, p)(t)\|_{\mathscr{E}}^2 - \|(\boldsymbol{u}_h, p_h)(t)\|_{\mathscr{E}_h}^2 \ge 0,$$
$$\|(\boldsymbol{u}, p)(t)\|_{\mathscr{E}}^2 - \|(\boldsymbol{u}_h, p_h)(t)\|_{\mathscr{E}_h}^2 \lesssim h^{2(k+1)} \left(|\boldsymbol{u}_0|_{k+1,\Omega_h}^2 + \widehat{c}^2\,|p_0|_{k+1,\Omega_h}^2 \right).$$

$\square$

5. Time integration

In the light of energy conservation (2.4) and (3.10) and the energy error estimate in Proposition 4.3, it is crucial to understand how the energy is preserved or not under time-stepping schemes.

In the present section we formulate a fully discrete version of Problem 3 aiming at preserving the energy of the system. Therefore, we introduce a sequence of time steps $t_n = n\tau$, $n = 0, \ldots, N$, with time step size τ. Next, we define $\boldsymbol{v}_{h,\tau}^n := \boldsymbol{v}_h(\cdot, t_n)$ (resp. $q_{h,\tau}^n := q_h(\cdot, t_n)$) as the approximation of the function $\boldsymbol{v}_h(\cdot, t) \in \boldsymbol{V}_k$ (resp. $q_h(\cdot, t) \in Q_k$) at time t_n, $n = 0, \ldots, N$. To integrate in time Problem 3, we take under consideration the family of θ-method schemes and analyse their energy conservation properties. The fully discrete systems consequently reads as follows:

Given $(\boldsymbol{u}_{h,\tau}^0, p_{h,\tau}^0) = (\Pi_k^0 \boldsymbol{u}_0, \Pi_k^0 p_0)$, find $(\boldsymbol{u}_{h,\tau}^n, p_{h,\tau}^n)$ for $n = 0, \ldots, N$ s.t.

$$
\begin{cases}
m_h\left(\dfrac{\boldsymbol{u}_{h,\tau}^{n+1} - \boldsymbol{u}_{h,\tau}^n}{\tau}, \boldsymbol{v}_h\right) + b(\boldsymbol{v}_h, \theta p_{h,\tau}^{n+1} + (1-\theta)p_{h,\tau}^n) + r(\theta \boldsymbol{u}_{h,\tau}^{n+1} + (1-\theta)\boldsymbol{u}_{h,\tau}^n, \boldsymbol{v}_h) = 0 & \forall \boldsymbol{v}_h \in \boldsymbol{V}_k, \\[1em]
n\left(\dfrac{p_{h,\tau}^{n+1} - p_{h,\tau}^n}{\tau}, q_h\right) - b(\theta \boldsymbol{u}_{h,\tau}^{n+1} + (1-\theta)\boldsymbol{u}_{h,\tau}^n, q_h) = \theta F^{n+1}(q_h) + (1-\theta)F^n(q_h) & \forall q_h \in Q_k,
\end{cases}
$$
$$(5.1)$$

where $F^n(q_h) := (f(t_n), q_h)_\Omega$ and $\theta \in [0,1]$. It is well known that all θ-methods are first order accurate in time, except for $\theta = 1/2$, i.e., the Crank-Nicolson method, which is second order accurate.

To analyse the energy conservation of the proposed schemes we consider null forcing terms, i.e. $f = 0$, and $\Gamma_R = \emptyset$. Thus, the above system reduces to

$$
\begin{cases}
m_h\left(\dfrac{\boldsymbol{u}_{h,\tau}^{n+1} - \boldsymbol{u}_{h,\tau}^n}{\tau}, \boldsymbol{v}_h\right) + b(\boldsymbol{v}_h, \theta p_{h,\tau}^{n+1} + (1-\theta)p_{h,\tau}^n) = 0 & \forall \boldsymbol{v}_h \in \boldsymbol{V}_k, \\[1em]
n\left(\dfrac{p_{h,\tau}^{n+1} - p_{h,\tau}^n}{\tau}, q_h\right) - b(\theta \boldsymbol{u}_{h,\tau}^{n+1} + (1-\theta)\boldsymbol{u}_{h,\tau}^n, q_h) = 0 & \forall q_h \in Q_k.
\end{cases}
$$
$$(5.2)$$

We start by considering in (5.2)

$$\boldsymbol{v}_h = \theta \boldsymbol{u}_{h,\tau}^{n+1} + (1-\theta)\boldsymbol{u}_{h,\tau}^n \in \boldsymbol{V}_k, \qquad \text{and} \qquad q_h = \theta p_{h,\tau}^{n+1} + (1-\theta)p_{h,\tau}^n \in Q_k,$$

and by summing together the two above equation we get

$$m_h\left(\frac{\boldsymbol{u}_{h,\tau}^{n+1} - \boldsymbol{u}_{h,\tau}^n}{\tau}, \theta \boldsymbol{u}_{h,\tau}^{n+1} + (1-\theta)\boldsymbol{u}_{h,\tau}^n\right) + n\left(\frac{p_{h,\tau}^{n+1} - p_{h,\tau}^n}{\tau}, \theta p_{h,\tau}^{n+1} + (1-\theta)p_{h,\tau}^n\right) = 0,$$

that is

$$\theta \|(\boldsymbol{u}_{h,\tau}^{n+1}, p_{h,\tau}^{n+1})\|_{\mathscr{E}_h}^2 + (1-2\theta)\left(m_h(\boldsymbol{u}_{h,\tau}^{n+1}, \boldsymbol{u}_{h,\tau}^n) + n(p_{h,\tau}^{n+1}, p_{h,\tau}^n)\right) = (1-\theta)\|(\boldsymbol{u}_{h,\tau}^n, p_{h,\tau}^n)\|_{\mathscr{E}_h}^2,$$

which, rearranging the terms, is

$$\|(\boldsymbol{u}_{h,\tau}^{n+1}, p_{h,\tau}^{n+1})\|_{\mathscr{E}_h}^2 + (2\theta - 1)\|(\boldsymbol{u}_{h,\tau}^{n+1} - \boldsymbol{u}_{h,\tau}^n, p_{h,\tau}^{n+1} - p_{h,\tau}^n)\|_{\mathscr{E}_h}^2 = \|(\boldsymbol{u}_{h,\tau}^n, p_{h,\tau}^n)\|_{\mathscr{E}_h}^2. \tag{5.3}$$

Now, it is easy to see that for $n = 0, \ldots, N$:

- if $\theta = 1/2$, i.e., for the Crank-Nicolson method, the discrete energy is conserved, i.e.

$$\|(\boldsymbol{u}_{h,\tau}^n, p_{h,\tau}^n)\|_{\mathscr{E}_h} = \|(\boldsymbol{u}_{h,\tau}^0, p_{h,\tau}^0)\|_{\mathscr{E}_h} = \|(\Pi_k^0 \boldsymbol{u}_0, \Pi_k^0 p_0)\|_{\mathscr{E}},$$

- if $1/2 < \theta \leq 1$, that is $2\theta - 1 > 0$, the second term in (5.3) is positive and then we can obtain

$$\|(\boldsymbol{u}_{h,\tau}^{n+1}, p_{h,\tau}^{n+1})\|_{\mathscr{E}_h}^2 \leq \|(\boldsymbol{u}_{h,\tau}^{n}, p_{h,\tau}^{n})\|_{\mathscr{E}_h}^2,$$

   that means dissipation of energy, cf. [46],
- if $0 \leq \theta < \frac{1}{2}$, that is $2\theta - 1 < 0$, the second term in (5.3) is negative and then we have

$$\|(\boldsymbol{u}_{h,\tau}^{n+1}, p_{h,\tau}^{n+1})\|_{\mathscr{E}_h}^2 \geq \|(\boldsymbol{u}_{h,\tau}^{n}, p_{h,\tau}^{n})\|_{\mathscr{E}_h}^2, \tag{5.4}$$

   that is the method produces a nondecreasing energy at each time step, in agreement with [47].

To obtain an explicit nearby energy-conservative scheme, one can consider, for example, the symplectic Euler scheme, that reduces to:

$$\begin{cases} n\left(\dfrac{p_{h,\tau}^{n+1} - p_{h,\tau}^{n}}{\tau}, q_h\right) - b(\boldsymbol{u}_{h,\tau}^{n}, q_h) = F^n(q_h) & \forall q_h \in Q_k, \\[3mm] m_h\left(\dfrac{\boldsymbol{u}_{h,\tau}^{n+1} - \boldsymbol{u}_{h,\tau}^{n}}{\tau}, \boldsymbol{v}_h\right) + b(\boldsymbol{v}_h, p_{h,\tau}^{n+1}) + r(\boldsymbol{u}_{h,\tau}^{n}, \boldsymbol{v}_h) = 0 & \forall \boldsymbol{v}_h \in \boldsymbol{V}_k. \end{cases} \tag{5.5}$$

We refer the reader to [52] for the analysis.

6. Numerical tests

In this section we provide some numerical examples to show the behaviour of the method and give numerical evidence of the theoretical results derived in the previous sections. We consider three test cases: the first in Subsection 6.1 presents the expected convergence rates for different approximation degree over several mesh families. The second test case, given in Subsection 6.2, is focused on the energy conservation properties of the scheme. Finally, in Subsection 6.3, we consider a wave propagation problem in a domain having with small curved inclusions. The latter is handled by using the extension of VEM to curved edges (cf. Remark 2).

6.1. *Error decay*

In this first test case, we verify the expected convergence rate of the method for different mesh families:

- `tria` a simplicial mesh;
- `quad` a Cartesian mesh;
- `hexa` composed by distorched hexagons;
- `voro` a mesh made of Voronoi cells optimized via a Lloyd algorithm.

In order to compute the VEM errors between the exact solution $(\boldsymbol{u}, p)$ and the VEM solution $(\boldsymbol{u}_h, p_h)$ at the final time T, we consider the computable L^2-like error quantities,

$$e_{\boldsymbol{u}} := \|\boldsymbol{u}(T) - \Pi_k^0 \boldsymbol{u}_h(T)\|_{0,\Omega} \quad \text{and} \quad e_p := \|p(T) - \Pi_k^0 p_h(T)\|_{0,\Omega}.$$

Let us set the mesh-size parameter

$$h := \frac{1}{L_P} \sum_{E \in \Omega_h} h_E.$$

For each family, we build a sequence of four meshes with decreasing mesh size h. In Figure 1 we depict one mesh as representative of each family.
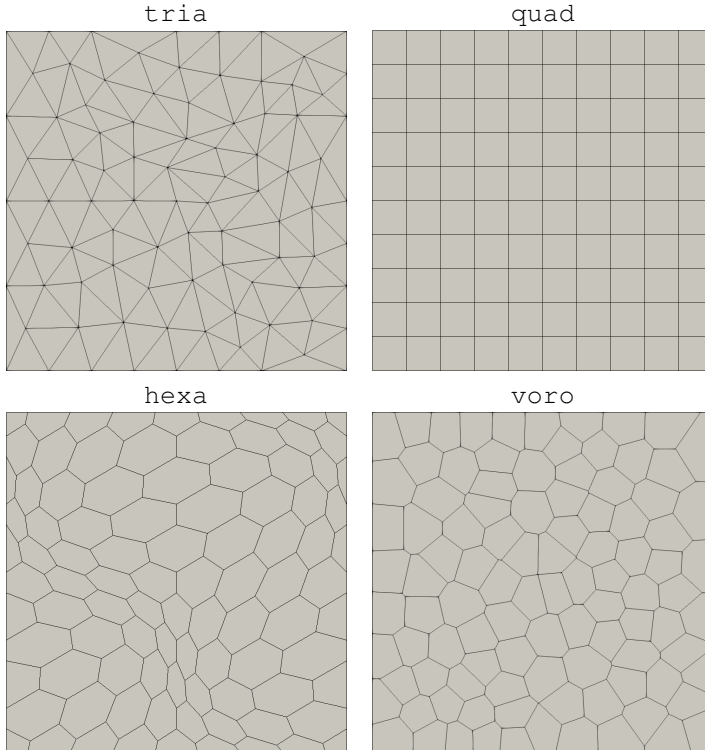

FIG. 1. Example of the adopted polygonal meshes. Example in Subsection 6.1.

In accordance with Proposition 4.2, the trend of each error indicator is computed and compared to the expected convergence trend. We consider a problem on $\Omega = (0,1)^2$ with analytical solution given by

$$\boldsymbol{u}(\boldsymbol{x},t) = \begin{bmatrix} -2\pi\cos(2\pi x)\cos(2\pi y)\sin(t) \\ 2\pi\sin(2\pi x)\sin(2\pi y)\sin(t) \end{bmatrix},$$

$$p(\boldsymbol{x},t) = \cos(2\pi y)\sin(2\pi x)\cos(t).$$

We set $\Gamma_D = \partial\Omega$, $\Gamma_N = \Gamma_R = \emptyset$ and choose $c = 1$. Boundary and initial conditions as well as the forcing term f in Problem 1 are computed accordingly. Since we are considering the space discretization error, we set $T = 1.e-7$ and $\tau = 1.e-8$ with $\theta = 1$ in (5.1).

The computed errors are given in Figure 2 and 3. Such convergence lines are coherent with the estimates derived in the theoretical results, see Proposition 4.2. For high approximation degree and fine mesh size, we notice stagnation of the error of the `hexa` and `voro` families. This is an expected behaviour discussed in [25]. A possible solution is to introduce a different basis for the polynomial expansion that makes the local systems better conditioned. However, this is out of the scope of the current work and it may be a good starting point for future investigations.
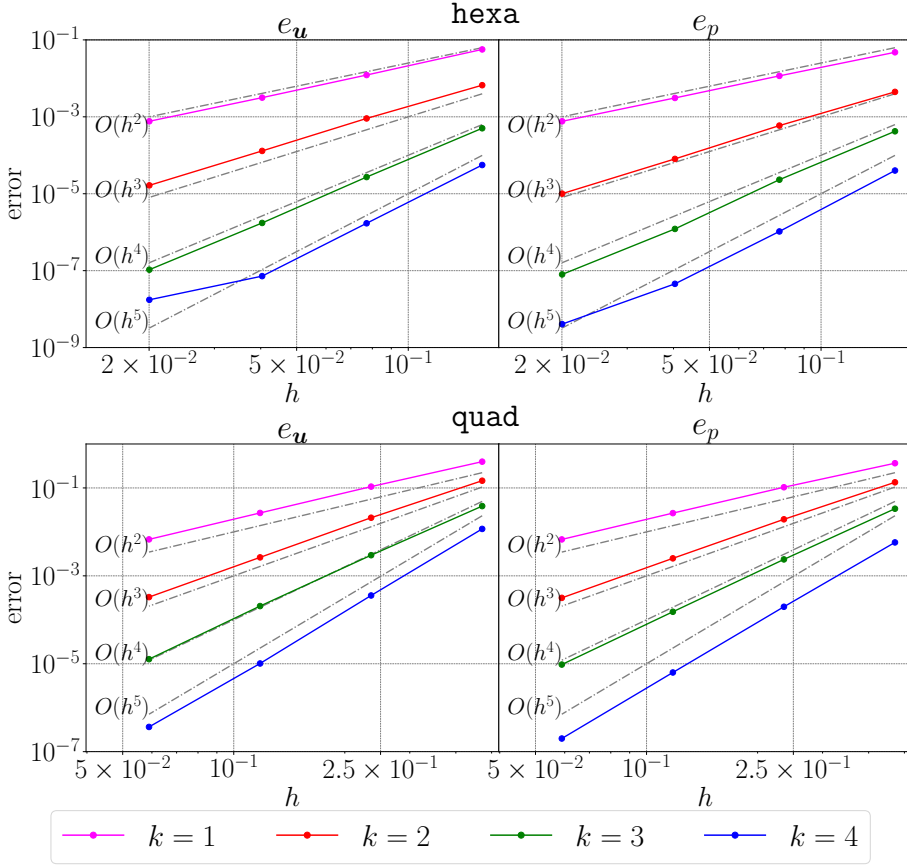
FIG. 2. Error decay for different type of meshes. Example in Subsection 6.1.

6.2. *Conservation of energy*

In this second example, we test the conservation of energy given, for the semi-discrete system, in (3.10). We consider the same mesh families and approximation degrees of the previous example and we choose four different time integration schemes: Explicit Euler, i.e. $\theta = 0$ in (5.2), Implicit Euler, i.e. $\theta = 1$ in (5.2) Crank-Nicolson, i.e. $\theta = \frac{1}{2}$ in (5.2), and Symplectic Euler (5.5). As observed in Section 3.4, the space discretization does locally conserve the energy so the possible lack of conservation will be due to the temporal scheme.

The spatial domain is still the unit square, $\Gamma_D = [0,1] \times \{0,1\}$ i.e. the top and the bottom boundaries, $\Gamma_N = \{0,1\} \times [0,1]$ i.e. the left and right boundaries, and $\Gamma_R = \emptyset$. The final time is $T = 1$ and $\tau = 1/200$. We set to zero the source term, the characteristic velocity $c = 1$ and the initial velocity and pressure as

$$\boldsymbol{u}(\boldsymbol{x},0) = \begin{bmatrix} \sin(x) \\ \cos(y) \end{bmatrix}, \quad \text{and} \quad p(\boldsymbol{x},0) = \cos(2\pi y)\sin(2\pi x).$$

The conservation of energy is depicted in Figure 4. In these graphs we compute the difference between the initial energy and the one at a specific time step and we report such values multiplied by a
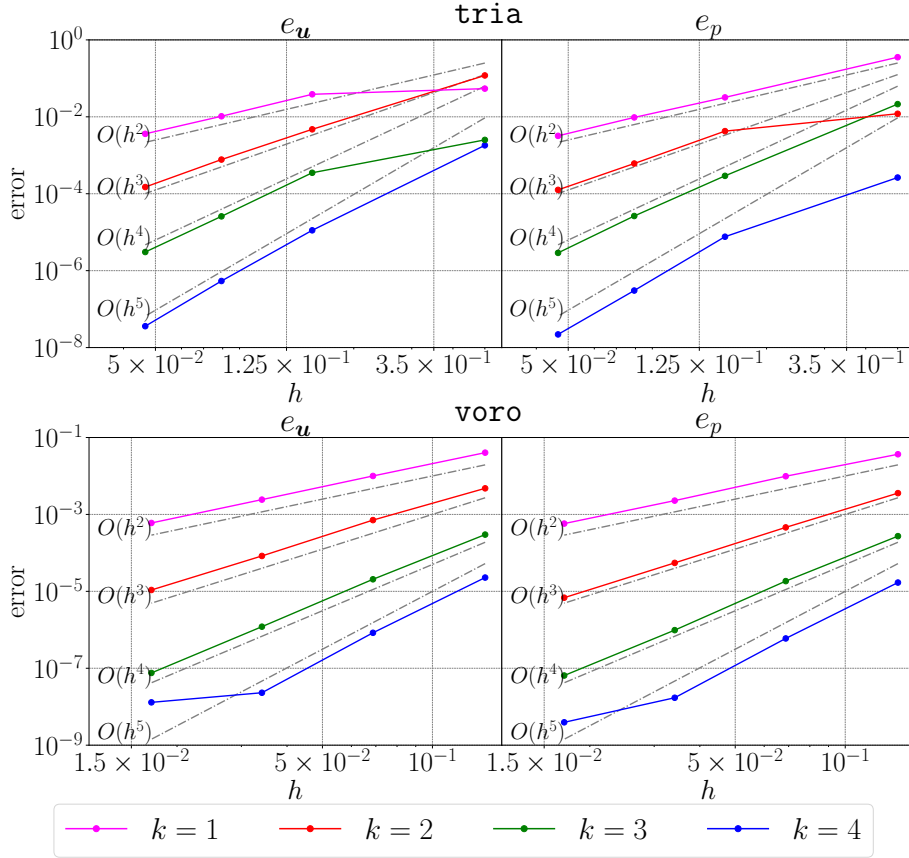
FIG. 3. Error decay for different type of meshes. Example in Subsection 6.1.

factor of 10^4. We notice that for the Explicit Euler the energy tends to increase during time in agreement with (5.4). This trend becomes more evident for higher approximation degree. For the Implicit Euler the situation has an opposite behaviour. Indeed, the energy is now dissipated during time. Also for this scheme, higher approximation degrees tend to dissipate more energy. The semi-implicit Symplectic Euler scheme mitigates this effect: the energy is not conserved during time, but the absolute error does not grow and stay limited. Finally, Crank-Nicolson shows a perfect energy conservation property. To better appreciate this behaviour we report in Table 1 the values

$$\mathrm{E} = \frac{\|(\boldsymbol{u}_{h,\tau}^T, p_{h,\tau}^T)\|_{\mathscr{E}_h} - \|(\boldsymbol{u}_{h,\tau}^0, p_{h,\tau}^0)\|_{\mathscr{E}_h}}{\|(\boldsymbol{u}_{h,\tau}^0, p_{h,\tau}^0)\|_{\mathscr{E}_h}}, \tag{6.1}$$

being $\|(\boldsymbol{u}_{h,\tau}^T, p_{h,\tau}^T)\|_{\mathscr{E}_h}$ the energy of the system at final time T. The behaviours of these time discretisation schemes perfectly match the arguments in Section 5.

E	tria	quad	hexa	voro
k = 1	7.4038e-16	8.6677e-15	2.0568e-15	9.0382e-15
k = 2	1.2555e-14	2.7043e-14	2.2665e-15	2.4104e-15
k = 3	2.8832e-14	2.2205e-13	6.3020e-16	1.0358e-14
k = 4	2.9968e-15	1.2107e-13	2.2041e-16	1.6068e-14

TABLE 1   *Energy errors* E *computed as in* (6.1) *for the Crank-Nicolson scheme in* (5.2).

6.3. *Multiple scattering in curved configurations*

In this example, we show the qualitative behaviour of the solution computed by the proposed approach in a domain with multiple circular inclusions. We consider two different configurations that are inspired by [12]. Both domain are defined in $\Omega = (0,1)^2$, but the first one has five holes whose centres are located at

$$\boldsymbol{x}_1 = [a,c]^\top, \quad \boldsymbol{x}_2 = [a,b]^\top, \quad \boldsymbol{x}_3 = [a,a]^\top, \quad \boldsymbol{x}_4 = [b,a]^\top, \quad \boldsymbol{x}_5 = [c,a]^\top,$$

while the second one has three additional circles centred at

$$\boldsymbol{x}_6 = [b,c]^\top, \quad \boldsymbol{x}_7 = [c,c]^\top, \quad \boldsymbol{x}_8 = [c,b]^\top,$$

where the values of the three parameters are given by

$$a = 0.6052631578947355, \quad b = 0.5, \quad \text{and} \quad c = 0.3947368421052622.$$

All circles have diameter 0.02. We refer to the first and the second case as `fiveHoles` and `eightHoles`, respectively. The grid is build starting from a structured quadrilateral mesh, where the cells intersecting with a circle are properly cut. Moreover, since we exploit the possibility to include the geometry information within VEM spaces [39], we do not need to over-refine edges to get an accurate representation of the circles themselves. As a consequence, we can reduce the computational effort without losing the accuracy of the solution, by neglecting spurious waves due to a piece-wise linear representation of the circles.

For both `fiveHoles` and `eightHoles` examples, we build two meshes, see Figure 5. The first one starting from a square divided in 38×38 uniform squares. Then, the second one is constructed by refining 2 times only the quadrilateral elements of the first one, see the detail in Figure 6.

Along the external boundaries of Ω, we impose absorbing boundary conditions, while on all the small circles perimeters we use homogeneous Neumann conditions. Then, we consider $c = 1$ and the following source term

$$f(\boldsymbol{x},t) = 10. \, e^{-(t-1)^2/\sigma_1} e^{-\|\boldsymbol{x}-\boldsymbol{x}_c\|^2/\sigma_2},$$

with $\sigma_1 = 0.01$ and $\sigma_2 = 0.00125$ and $\boldsymbol{x}_c = [0.5, 0.5]^\top$. The initial values of both $\boldsymbol{u}$ and p are set to zero. We assume approximation degree equal to $k = 2$. As final time we take $T = 10$, we divide the interval $[0,T]$ into 50 equally spaced sub-intervals and we use the Crank-Nicolson time integration scheme.

In Figure 7 we show the computed pressure solution p_h evaluated at quadrature points at different time steps for the `fiveHoles` case. On the top panels we show the coarse mesh while, on the bottom
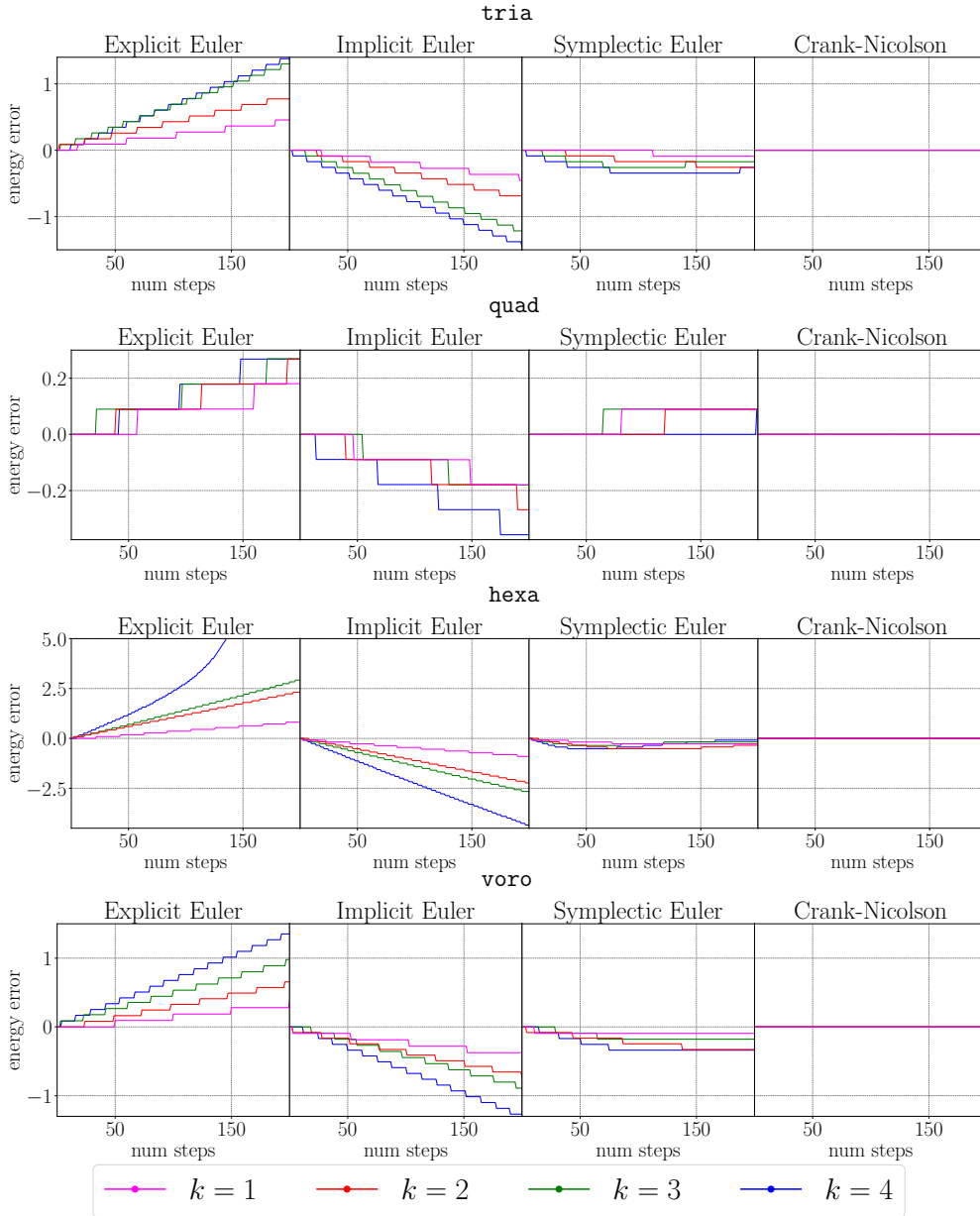
FIG. 4. Energy error for different schemes. For visualization purposes the values have been magnified by a factor 10^4. Example in Subsection 6.2.

ones, we consider the fine mesh. From a qualitative point of view we observe no much difference between them.
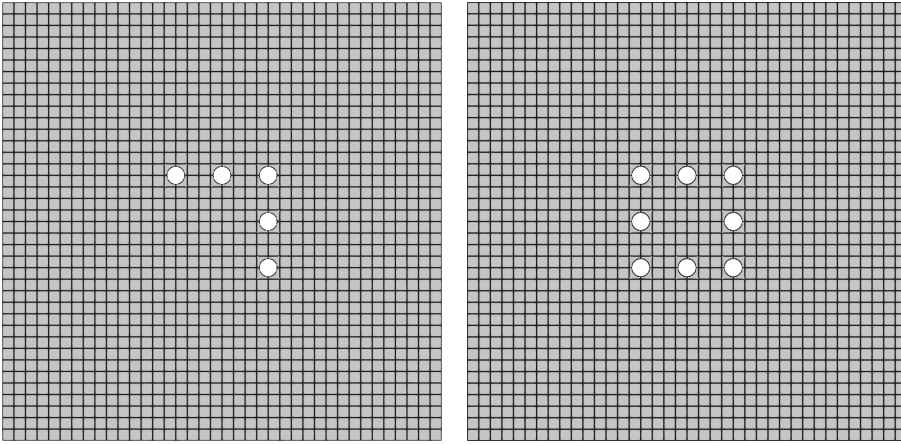
FIG. 5. Representation of the computational grid for `fiveHoles` (left) for `eightHoles` (right). Example in Subsection 6.3.
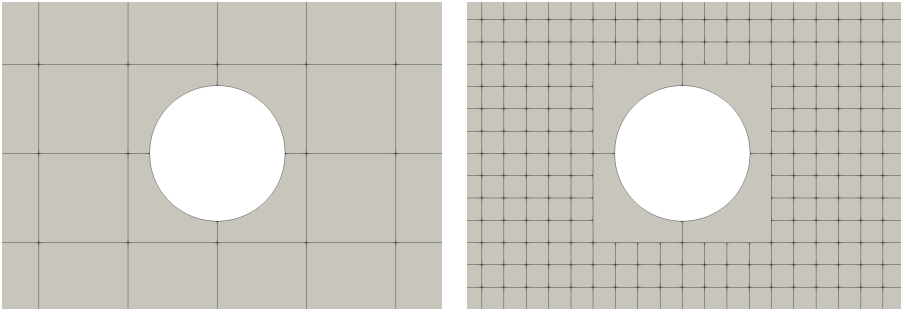

FIG. 6. Detail of one hole in the inital mesh (left) and in the refined one (right). Example in Subsection 6.3.

In Figure 8 we consider the `eightHoles` case. Also for this experiment we observe that the coarser mesh provides similar results of the ones obtained with the refined mesh. Moreover, since the holes are displaced in a symmetric way with respect to $\boldsymbol{x}_c$ we expect the waves preserve a symmetric structure. This is confirmed by the snapshots represented in Figure 8.

7. Conclusions

In this work, we presented a general order virtual element numerical discretization scheme to approximate the wave equation written in mixed form. The latter results in a first order system of differential equations in both space and time dimension. We presented the *a-priori* stability analysis as well as the convergence property of the scheme in a suitable energy norm and we showed that the proposed virtual element scheme preserve the semi-discrete energy of the system in absence of external load. To integrate in time the semi-discrete problem we consider the family of the θ - method schemes and we discuss their energy conservation properties. We verified the theoretical results on different benchmark tests and we applied the proposed scheme on a domain with circular inclusions to show the capabilities of the method in term of accuracy and of flexibility in handling complex geometries. To conclude, the presented mixed virtual element method allows a robust and flexible numerical

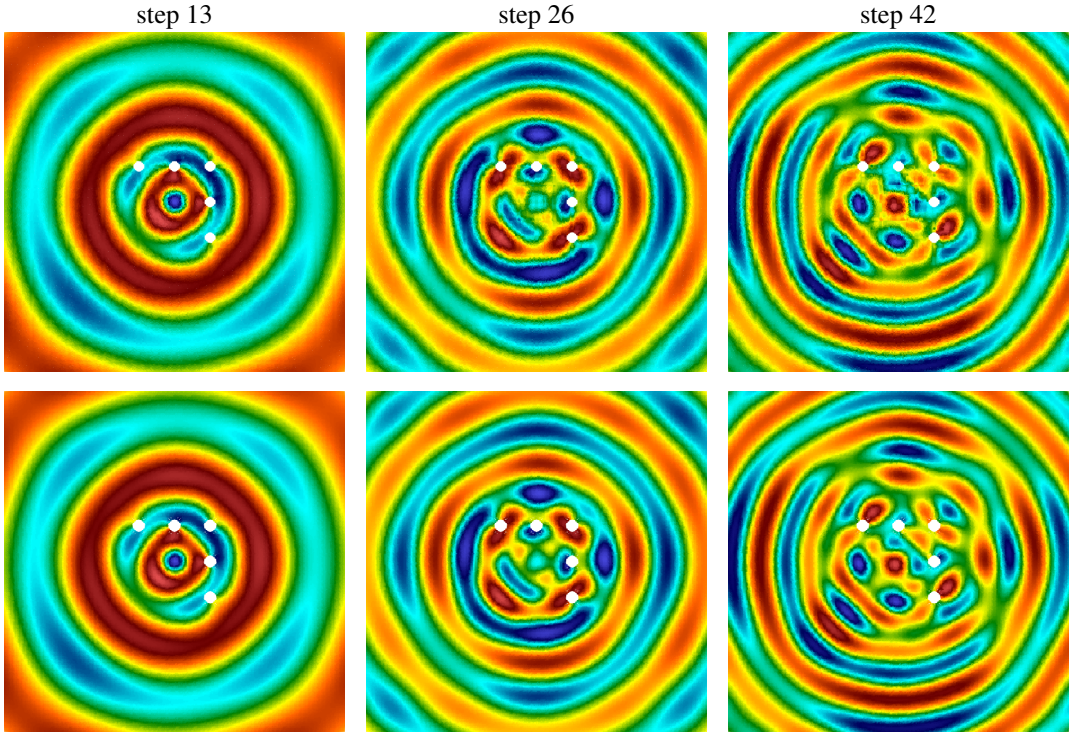step 13   step 26   step 42

FIG. 7. Solution obtained with the `fiveHoles` mesh, on the top with a coarse grid and on the bottom with a finer grid. Example in Subsection 6.3.

discretization that can be successfully applied to wave propagation problems. Future developments in this direction may include the study of multi-physics problems (written in a mixed form) such as vibro-acoustics (with elastic or poroelastic structure) interaction problems.

Acknowledgments

REFERENCES

1. R. A. Adams. *Sobolev spaces*. Pure and Applied Mathematics, Vol. 65. Academic Press, New York-London, 1975.
2. P. F. Antonietti, L. Beirão da Veiga, S. Scacchi, and M. Verani. A C^1 virtual element method for the Cahn-Hilliard equation with polygonal meshes. *SIAM J. Numer. Anal.*, 54(1):34–56, 2016.
3. P. F. Antonietti, F. Bonaldi, and I. Mazzieri. A high-order discontinuous Galerkin approach to the elasto-acoustic problem. *Comput. Methods Appl. Mech. Engrg.*, 358:112634, 29, 2020.
4. P. F. Antonietti, G. Manzini, I. Mazzieri, H. M. Mourad, and M. Verani. The arbitrary-order virtual element method for linear elastodynamics models: convergence, stability and dispersion-dissipation analysis. *Internat.*
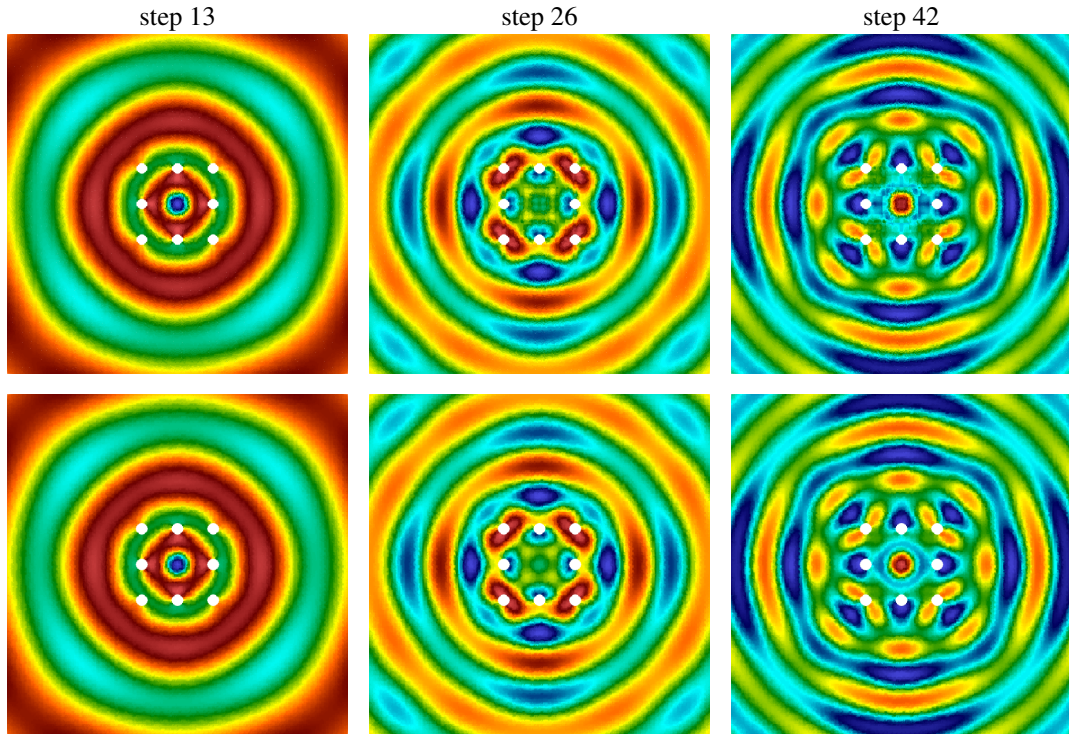
step 13   step 26   step 42

FIG. 8. Solution obtained with the `eightHoles` mesh, on the top with a coarse grid and on the bottom with a finer grid. Example in Subsection 6.3.

J. Numer. Methods Engrg., 122(4):934–971, 2021.

5. P. F. Antonietti, C. Marcati, I. Mazzieri, and A. Quarteroni. High order discontinuous Galerkin methods on simplicial elements for the elastodynamics equation. *Numer. Algorithms*, 71(1):181–206, 2016.

6. P. F. Antonietti and I. Mazzieri. High-order discontinuous Galerkin methods for the elastodynamics equation on polygonal and polyhedral meshes. *Comput. Methods Appl. Mech. Engrg.*, 342:414–437, 2018.

7. P. F. Antonietti, I. Mazzieri, M. Muhr, V. Nikolić, and B. Wohlmuth. A high-order discontinuous Galerkin method for nonlinear sound waves. *J. Comput. Phys.*, 415:109484, 27, 2020.

8. P. F. Antonietti, I. Mazzieri, A. Quarteroni, and F. Rapetti. Non-conforming high order approximations of the elastodynamics equation. *Comput. Methods Appl. Mech. Engrg.*, 209/212:212–238, 2012.

9. D. N. Arnold, D. Boffi, and R. S. Falk. Quadrilateral $H(\text{div})$ finite elements. *SIAM J. Numer. Anal.*, 42(6):2429–2451, 2005.

10. E. Artioli, S. de Miranda, C. Lovadina, and L. Patruno. A stress/displacement virtual element method for plane elasticity problems. *Comput. Methods Appl. Mech. Engrg.*, 325:155–174, 2017.

11. P. Bansal, A. Moiola, I. Perugia, and C. Schwab. Space-time discontinuous Galerkin approximation of acoustic waves with point singularities. *IMA J. Numer. Anal.*, 41(3):2056–2109, 2021.

12. Hélène Barucq, Julien Diaz, Vanessa Mattesi, and Sebastien Tordeux. Asymptotic behavior of acoustic waves scattered by very small obstacles. *ESAIM: Mathematical Modelling and Numerical Analysis*, 55:S705–S731, 2021.

13. E. Bécache, P. Joly, and C. Tsogka. An analysis of new mixed finite elements for the approximation of wave propagation problems. *SIAM J. Numer. Anal.*, 37(4):1053–1084, 2000.

14. L. Beirão da Veiga, F. Brezzi, A. Cangiani, G. Manzini, L. D. Marini, and A. Russo. Basic principles of virtual element methods. *Math. Models Methods Appl. Sci.*, 23(1):199–214, 2013.

15. L. Beirão da Veiga, F. Brezzi, L. D. Marini, and A. Russo. $H(\text{div})$ and $H(\boldsymbol{curl})$-conforming virtual element methods. *Numer. Math.*, 133(2):303–332, 2016.

16. L. Beirão da Veiga, F. Brezzi, L. D. Marini, and A. Russo. Mixed virtual element methods for general second order elliptic problems on polygonal meshes. *ESAIM Math. Model. Numer. Anal.*, 50(3):727–747, 2016.

17. L. Beirão da Veiga, F. Brezzi, L. D. Marini, and A. Russo. Virtual element implementation for general elliptic equations. In *Building bridges: connections and challenges in modern approaches to numerical partial differential equations*, volume 114 of *Lect. Notes Comput. Sci. Eng.*, pages 39–71. Springer, [Cham], 2016.

18. L. Beirão da Veiga, F. Dassi, G. Manzini, and L. Mascotto. Virtual elements for Maxwell's equations. *Comput. Math. Appl.*, 116:82–99, 2022.

19. L. Beirão da Veiga, L. Lopez, and G. Vacca. Mimetic finite difference methods for Hamiltonian wave equations in 2D. *Comput. Math. Appl.*, 74(5):1123–1141, 2017.

20. L. Beirão da Veiga, C. Lovadina, and G. Vacca. Divergence free virtual elements for the Stokes problem on polygonal meshes. *ESAIM Math. Model. Numer. Anal.*, 51(2):509–535, 2017.

21. L. Beirão da Veiga, C. Lovadina, and G. Vacca. Virtual elements for the Navier-Stokes problem on polygonal meshes. *SIAM J. Numer. Anal.*, 56(3):1210–1242, 2018.

22. L. Beirão da Veiga, A. Russo, and G. Vacca. The virtual element method with curved edges. *ESAIM Math. Model. Numer. Anal.*, 53(2):375–404, 2019.

23. L. Beirão da Veiga and G. Vacca. Sharper Error Estimates for Virtual Elements and a Bubble-Enriched Version. *SIAM J. Numer. Anal.*, 60(4):1853–1878, 2022.

24. L. Beirão da Veiga, C. Lovadina, and A. Russo. Stability analysis for the virtual element method. *Math. Mod.and Meth. in Appl. Sci.*, 27(13):2557–2594, 2017.

25. S. Berrone and A. Borio. Orthogonal polynomials in badly shaped polygonal elements for the virtual element method. *Finite Elem. Anal. Des.*, 129:14–31, 2017.

26. D. Boffi, F. Brezzi, and M. Fortin. *Mixed finite element methods and applications*, volume 44 of *Springer Series in Computational Mathematics*. Springer, Heidelberg, 2013.

27. D. Boffi, F. Brezzi, and M. Fortin. *Mixed finite element methods and applications*, volume 44 of *Springer Series in Computational Mathematics*. Springer, Heidelberg, 2013.

28. S. C. Brenner, Q. Guan, and L. Y. Sung. Some estimates for virtual element methods. *Comput. Methods Appl. Math.*, 17(4):553–574, 2017.

29. S. C. Brenner and L. R. Scott. *The mathematical theory of finite element methods*, volume 15 of *Texts in Applied Mathematics*. Springer, New York, third edition, 2008.

30. F. Brezzi, J Douglas, R. Durán, and M. Fortin. Mixed finite elements for second order elliptic problems in three variables. *Numer. Math.*, 51(2):237–250, 1987.

31. F. Brezzi, J. Douglas, and L. D. Marini. Two families of mixed finite elements for second order elliptic problems. *Numer. Math.*, 47(2):217–235, 1985.

32. E. Burman, O. Duran, and A. Ern. Hybrid high-order methods for the acoustic wave equation in the time domain. *Commun. Appl. Math. Comput.*, 4(2):597–633, 2022.

33. A. Chernov, C. Marcati, and L. Mascotto. *p*- and *hp*-virtual elements for the Stokes problem. *Adv. Comput. Math.*, 47(2):Paper No. 24, 31, 2021.

34. E. T. Chung and B. Engquist. Optimal discontinuous Galerkin methods for wave propagation. *SIAM J. Numer. Anal.*, 44(5):2131–2158, 2006.

35. E. T. Chung and B. Engquist. Optimal discontinuous Galerkin methods for the acoustic wave equation in higher dimensions. *SIAM J. Numer. Anal.*, 47(5):3820–3848, 2009.

36. B. Cockburn and V. Quenneville-Bélair. Uniform-in-time superconvergence of the HDG methods for the acoustic wave equation. *Math. Comp.*, 83(285):65–85, 2014.

37. G. Cohen, P. Joly, J. E. Roberts, and N. Tordjman. Higher order triangular finite elements with mass lumping for the wave equation. *SIAM J. Numer. Anal.*, 38(6):2047–2078, 2001.

38. L. C. Cowsar, T. F. Dupont, and M. F. Wheeler. A priori estimates for mixed finite element methods for the wave equation. *Comput. Methods Appl. Mech. Eng.*, 82(1-3):205–222, 1990.

39. F. Dassi, A. Fumagalli, D. Losapio, S. Scialò, A. Scotti, and G. Vacca. The mixed virtual element method on curved edges in two dimensions. *Comput. Methods Appl. Mech. Engrg.*, 386:Paper No. 114098, 25, 2021.

40. F. Dassi, A. Fumagalli, I. Mazzieri, A. Scotti, and G. Vacca. A virtual element method for the wave equation on curved edges in two dimensions. *J. Sci. Comput.*, 90(1):Paper No. 50, 25, 2022.

41. F. Dassi, A. Fumagalli, A. Scotti, and G. Vacca. Bend 3d mixed virtual element method for Darcy problems. *Comput. Math. Appl.*, 119:1–12, 2022.

42. J. D. De Basabe and M. K. Sen. Stability of the high-order finite elements for acoustic or elastic wave propagation with high-order time stepping. *Geophys. J. Int.*, 181(1):577–590, 2010.

43. J. D. De Basabe, M. K. Sen, and M. F Wheeler. The interior penalty discontinuous Galerkin method for elastic wave propagation: grid dispersion. *Geophys. J. Int.*, 175(1):83–93, 2008.

44. S. Delcourte and N. Glinsky. Analysis of a high-order space and time discontinuous Galerkin method for elastodynamic equations. Application to 3D wave propagation. *ESAIM Math. Model. Numer. Anal.*, 49(4):1085–1126, 2015.

45. H. Egger and B. Radu. Super-convergence and post-processing for mixed finite element approximations of the wave equation. *Numer. Math.*, 140(2):427–447, 2018.

46. T. Geveci. On the application of mixed finite element methods to the wave equations. *RAIRO Modél. Math. Anal. Numér.*, 22(2):243–250, 1988.

47. R. Glowinski and T. Rossi. A mixed formulation and exact controllability approach for the computation of the periodic solutions of the scalar wave equation. I. Controllability problem formulation and related iterative solution. *C. R. Math. Acad. Sci. Paris*, 343(7):493–498, 2006.

48. M. J. Grote, A. Schneebeli, and D. Schötzau. Discontinuous Galerkin finite element method for the wave equation. *SIAM J. Numer. Anal.*, 44(6):2408–2431, 2006.

49. L. He, F. Wang, and J. Wen. A mixed discontinuous Galerkin method for the wave equation. *Comput. Math. Appl.*, 82:60–73, 2021.

50. E. W. Jenkins. Numerical solution of the acoustic wave equation using Raviart-Thomas elements. *J. Comput. Appl. Math.*, 206(1):420–431, 2007.

51. E. W. Jenkins, B. Rivière, and M. F. Wheeler. A priori error estimates for mixed finite element approximations of the acoustic wave equation. *SIAM J. Numer. Anal.*, 40(5):1698–1715, 2002.

52. R. C. Kirby and T. T. Kieu. Symplectic-mixed finite element approximation of linear acoustic wave equations. *Numer. Math.*, 130(2):257–291, 2015.

53. L. Mascotto, I. Perugia, and A. Pichler. A nonconforming Trefftz virtual element method for the Helmholtz problem. *Math. Models Methods Appl. Sci.*, 29(9):1619–1656, 2019.

54. E. D. Mercerat and N. Glinsky. A nodal high-order discontinuous Galerkin method for elastic wave propagation in arbitrary heterogeneous media. *Geophys. J. Int.*, 201(2):1101–1118, 2015.

55. P. Monk and G. R. Richter. A discontinuous Galerkin method for linear symmetric hyperbolic systems in inhomogeneous media. *J. Sci. Comput.*, 22/23:443–477, 2005.

56. J.-C. Nédélec. A new family of mixed finite elements in $\mathbf{R}^3$. *Numer. Math.*, 50(1):57–81, 1986.

57. A. Quarteroni and A. Valli. *Numerical approximation of partial differential equations*, volume 23 of *Springer Series in Computational Mathematics*. Springer-Verlag, Berlin, 1994.

58. P.-A. Raviart and J.-M. Thomas. A mixed finite element method for 2nd order elliptic problems. In *Mathematical aspects of finite element methods (Proc. Conf., Consiglio Naz. delle Ricerche (C.N.R.), Rome, 1975)*, Lecture Notes in Math., Vol. 606, pages 292–315. Springer, Berlin, 1977.

59. B. Rivière, S. Shaw, and J. R. Whiteman. Discontinuous Galerkin finite element methods for dynamic linear solid viscoelasticity problems. *Numer. Methods Partial Differential Equations*, 23(5):1149–1166, 2007.

60. B. Rivière and M. F. Wheeler. Discontinuous finite element methods for acoustic and elastic wave problems. In *Current trends in scientific computing (Xi'an, 2002)*, volume 329 of *Contemp. Math.*, pages 271–282. American Mathematical Society, 2003.

61. J. E. Roberts and J.-M. Thomas. Mixed and hybrid methods. In *Handbook of numerical analysis, Vol. II*, Handb. Numer. Anal., II, pages 523–639. North-Holland, Amsterdam, 1991.

62. G. Vacca. Virtual element methods for hyperbolic problems on polygonal meshes. *Comput. Math. Appl.*, 74(5):882–898, 2017.

MOX Technical Reports, last issues

Dipartimento di Matematica
Politecnico di Milano, Via Bonardi 9 - 20133 Milano (Italy)

63/2022   Corti, M.; Antonietti, P.F.; Dede', L.; Quarteroni, A.
Numerical Modelling of the Brain Poromechanics by High-Order Discontinuous Galerkin Methods

64/2022   Massi, M.C., Dominoni, L., Ieva, F., Fiorito, G.
A Deep Survival EWAS approach estimating risk profile based on pre-diagnostic DNA methylation: an application to Breast Cancer time to diagnosis

61/2022   Gregorio, C.; Cappelletto, C.; Romani, S.; Stolfo, D.; Merlo, M.; Barbati, G.
Using marginal structural joint models to estimate the effect of a time-varying treatment on recurrent events and survival: An application on arrhythmogenic cardiomyopathy

62/2022   Ciaramella, G.; Halpern, L.; Mechelli, L.
Convergence analysis and optimization of a Robin Schwarz waveform relaxation method for periodic parabolic optimal control problems

59/2022   Boon, W. M.; Fumagalli, A.
A multipoint vorticity mixed finite element method for incompressible Stokes flow

60/2022   Cortellessa, D.; Ferro, N.; Perotto, S.; Micheletti, S.
Enhancing level set-based topology optimization with anisotropic graded meshes

58/2022   Zingaro, A.; Bucelli, M.; Fumagalli, I.; Dede', L; Quarteroni, A.
Modeling isovolumetric phases in cardiac flows by an Augmented Resistive Immersed Implicit Surface Method

57/2022   Ruffino, L.; Santoro, A.; Sparvieri, S.; Regazzoni, F.; Adebo, D.A.; Quarteroni, A.; Vergara, C
Computational analysis of cardiovascular effects of COVID- 19 infection in children

55/2022   Cavinato, L.; Pegoraro, M.; Ragni, A.; Ieva, F.
Imaging-based representation and stratification of intra-tumor Heterogeneity via tree-edit distance

54/2022   Bucelli, M.; Zingaro, A.; Africa, P. C.; Fumagalli, I.; Dede', L.; Quarteroni, A.
A mathematical model that integrates cardiac electrophysiology, mechanics and fluid dynamics: application to the human left heart